RSC Advances

COMMUNICATION

View Article Online
View Journal | View Issue

Cite this: *RSC Adv.*, 2014, **4**, 37714

Salt-confinement enables production of nitrogen-doped porous carbons in an air oven†

Martina Ambrogi,[a] Yongjun Men,[a] Frank Polzer[b] and Jiayin Yuan*[a]

Received 9th July 2014
Accepted 4th August 2014

DOI: 10.1039/c4ra06886f

www.rsc.org/advances

The production of nitrogen-doped porous carbons in an air oven at 750 °C with high surface area (≥500 $m^2 g^{-1}$), carbonization yield up to 35 wt% and tuneable nitrogen content from ionic liquids was reported. It utilized inorganic halide salts as the reaction medium, the activation agents, and the physical barrier. This method was successfully expanded to recyclable sea salt and natural sources, such as nucleobase (adenine) and biomass (oak leaves).

1. Introduction

Nitrogen-doped porous carbons have attracted considerable interest in the past decade due to their unique physical and chemical properties and a wide application scope in the fields of catalysis, environment techniques and energy generation and storage.[1,2] The doping of nitrogen atoms in the carbon framework is well known to adjust the physical properties of carbon materials by increasing the overall electron density at the Fermi level, which improves the electric conductivity and oxidation stability.[3,4] In addition, nitrogen doping enhances the basicity of carbons and makes them highly attractive for catalytic applications, for example, methanol oxidation, anchoring of catalytically active metal nanoparticles, and oxygen reduction reactions, only to name a few.[5–14] Meanwhile, the unusual benefit received *via* nitrogen doping in carbons can be further amplified in a porous configuration that bears a high surface area to accelerate the mass/energy transport and boost their materials performance in electrochemical devices, such as lithium-ion batteries, electrochemical double layer capacitors and fuel cells.[2,14,15]

Two fundamental synthetic approaches to introduce nitrogen into carbons can be distinguished, the thermal treatment of carbon or its precursor under ammonia, or the straightforward carbonization of nitrogen-rich precursors.[1,16–21] The former deposits nitrogen atoms preferentially on the carbon surface, while the latter provides incorporation of structural nitrogen atoms into the bulk. Independent of the choice of these two methods, production of nitrogen-doped porous carbon under an oxygen-poor atmosphere is considered as a prerequisite, since the presence of oxygen at the carbonization temperature (typically 600 °C or above) will heavily attack the carbon product and turn it into gaseous compounds, usually CO or CO_2. This oxidation effect is much strengthened for porous carbons, where enormous surface area is available to undergo and accelerate the oxidation reaction. A literature survey indicates that the production of porous carbons with high specific surface area, S_{BET} (≥500 $m^2 g^{-1}$) directly in air is a rare case, not to mention the possible doping of nitrogen. Stucky *et al.* reported recently that an ultrasonic spray pyrolysis method with consecutive thermal treatment of confined core–shell microparticles could create porous carbon microspheres (nitrogen-free). In this case the porous carbon core of micrometer size was confined and protected by a thin, dense TiO_2 shell for the pyrolysis in air.[22] However, the necessity of particular equipment, complex design of the core–shell morphology, and the post-synthesis treatment to etch the TiO_2 scaffold limits the advantage of this process over the common preparation methods under inert atmosphere.[23] In fact not only the noble gas as protecting atmosphere but also the engineering setups increase the final production cost and complexity. From this point of view, production of nitrogen-doped porous carbons bearing a high S_{BET} without noble gas protection is not only scientifically challenging but also of practical values.

In this work a sustainable and easy-to-operate method to produce porous nitrogen-doped carbon materials in air *via* a salt-assisted approach is demonstrated. Specifically speaking, common inorganic halide salts, NaCl and $ZnCl_2$ were employed as the high-temperature ionic solvent, the activation agents to introduce pores into carbons, and the protecting barrier to confine a local oxygen-poor environment. Very interestingly this concept can be straightforward extended to natural sources,

[a]*Department of Colloid Chemistry Max Planck Institute of Colloids and Interfaces Am Mühlenberg 1, D-14476 Potsdam, Germany. E-mail: jiayin.yuan@mpikg.mpg.de*
[b]*Materials Science & Engineering University of Delaware, 217C Du Pont Hall, 19716 Newark, USA*

† Electronic supplementary information (ESI) available. See DOI: 10.1039/c4ra06886f

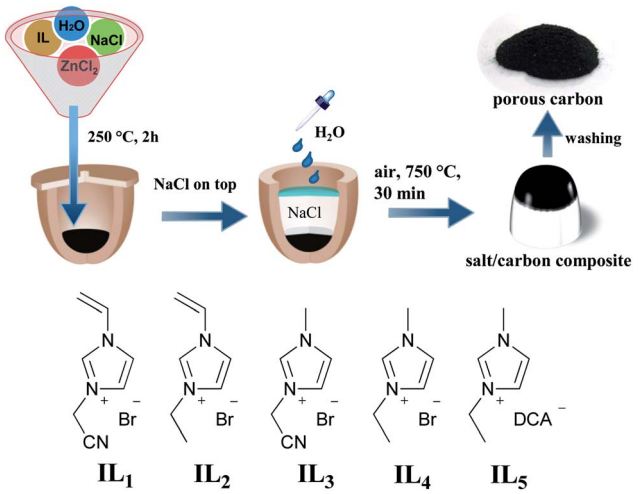

Fig. 1 Schematic representation of the carbonization process in an air oven. The chemical structures of the used ILs are illustrated beneath. DCA represents the dicyanamide anion.

such as sea salt as reaction medium, and nucleobase or oak leaves as carbon precursor. The general synthetic route is illustrated in Fig. 1.

2. Experimental

2.1 Materials

All chemicals were used as supplied. Reagents for the syntheses of IL_4 and IL_5 were purchased from IoLiTec company, and the rest were synthesized by ourselves according to our previous route.[24] The salts NaCl (99%) and $ZnCl_2$ (99%) were purchased from Sigma-Aldrich. All solvents used were of analytic grade. Ultrapure Milli-Q water was used in all experiments. Oak leaves were collected from a thicket located in Potsdam, Germany.

2.2 Synthesis of nitrogen-doped porous carbon from ILs

In a general procedure 1.5 g of carbon precursors was mixed with salt combination of NaCl and $ZnCl_2$ or Red Sea salt in a defined weight ratio listed in Table 1. The starting mixture was dissolved in 6 ml of water in a porcelain crucible, heating at 60 °C for 15 minutes under stirring. The sample was heated up to 250 °C (heating rate 4 °C min^{-1}) in air oven and the temperature was maintained stable for 2 hours. Afterwards the sample was directly covered with NaCl or sea salt (roughly 60 g). 3 ml of water were dropped on the surface in order to melt a thin layer of salt and then let it evaporate at room temperature for 30 minutes. The sample was placed in an air oven previously heated at 750 °C for the desired time and after that the sample was pulled out of the oven and cooled down to room temperature. The salt was then simply dissolved in water and the resulting carbon was treated with 1 N HCl aqueous solution for two days in order to remove final impurities from the pores. The product was separated by centrifugation and washed several times with water until neutral pH and then with mixtures of water–ethanol. The as-prepared carbon material was finally dried under vacuum at 80 °C overnight.

2.3 Synthesis of nitrogen-doped porous carbon from IL_1 under N_2 flow, with and without ceiling

The mixture of IL_1 : $ZnCl_2$: NaCl (weight ratio of 1 : 0.3 : 1) in water was dried in air oven at 250 °C for 2 hours, and the resulting carbonaceous matrix was then covered with fined grinded NaCl. The starting material was placed in the oven at room temperature and flushed with nitrogen flow for one hour before starting the heating in order to avoid eventually oxidation reactions during thermal treatment. The temperature was then increased with a heating rate of 10 °C min^{-1} up to 750 °C and the sample was held at this temperature for 30 minutes. After the treatment the sample was left inside the chamber until the temperature was cooled down naturally. The same purification procedure as the carbon produced in air oven was performed (see Section 2.2). When carbonization under nitrogen without NaCl ceiling on the top was performed, the procedure is exactly the same, except the sample was directly carbonized after the drying process (heating rate 10 °C min^{-1}, holding time 30 minutes).

2.4 Synthesis of nitrogen-doped porous carbon from adenine

We used the same procedure reported in Section 2.2 with adenine instead of IL. The weight ratio is adenine : $ZnCl_2$: NaCl = 1 : 0.3 : 1.

2.5 Synthesis of porous carbon from oak leaves and red sea salt

Oak leaves were firstly washed with water and then dried at 80 °C overnight. After grinded 1.5 g of leaves, a 1 : 1 weight ratio of sea salt was added and mixed carefully. The solid mixture was transferred into a crucible and fresh sea salt (roughly 60 g) was used to generate the confinement. 3 ml of water were dropped on the surface to melt a thin layer of salt and then it was dried at room temperature for 30 minutes. The sample was then placed directly at 750 °C in air oven for 30 minutes. The work-up of the product purification was the same as reported for ILs (see Section 2.2).

2.6 Characterization methods

Nitrogen sorption measurements were performed on Quantachrome Autosorb-1 at 77 K (liquid nitrogen temperature). Samples were degassed prior to the measurements at 150 °C for 20 hours. The specific surface area is calculated according to the Brunauer–Emmett–Teller (BET) equation, while quenched solid density functional theory (QSDFT) for cylindrical pores is applied for the evaluation of pore size distribution. This latter method takes in consideration the surface roughness and heterogeneity of the material, representing a more precise and realistic model for the surface area interpretation here. Combustion elemental analysis (C/H/N content) was carried out for all samples using Vario Micro setup (version 1.4.1). Thermal

Table 1 Characterization of nitrogen-doped porous carbons prepared *via* carbonization in an air oven under different reaction conditions. The EA results were obtained from the combustion EA analysis

Entry	Sample	S_{BET} (m^2 g^{-1})	Pore volume (cm^3 g^{-1})	Yield (wt%)	C (wt%)	N (wt%)	H (wt%)
1	$IL_1Z_0S_1T_{30}$	207	0.094	20.6	74.2	13.4	1.9
2	$IL_1Z_{0.1}S_1T_{30}$	412	0.172	31.2	68.0	13.5	2.3
3	$IL_1Z_{0.3}S_1T_{30}$	950	0.453	29.4	68.5	15.2	2.5
4	$IL_1Z_{0.5}S_1T_{30}$	811	0.690	28	71.1	13.6	2.4
5	$IL_1Z_{0.75}S_1T_{30}$	886	0.695	19.8	67.3	13.9	2.9
6	IL_1Z_1 S_1T_{30}	894	0.588	8.4	67.7	12.0	2.6
7	$IL_1Z_{0.3}S_0T_{30}$	419	0.186	34.3	64.2	14.9	2.5
8	$IL_1Z_{0.3}S_{0.3}T_{30}$	809	0.391	31.5	67.2	15.4	2.6
9	$IL_1Z_{0.3}S_{0.6}T_{30}$	747	0.538	31.9	68.2	15.4	2.7
10	$IL_1Z_{0.3}S_2T_{30}$	805	0.397	33.1	67.1	16.0	2.9
11	$IL_1Z_{0.3}S_1T_{15}$	812	0.477	28.3	64.5	15.3	2.7
12	$IL_1Z_{0.3}S_1T_{60}$	990	0.569	19.3	68.2	12.3	2.6
13	$IL_1Z_{0.3}S_1T_{120}$	1130	0.692	8.4	70.6	10.6	2.4
14	$IL_2Z_{0.3}S_1T_{30}$	502	0.273	11.5	67.6	12.7	2.3
15	$IL_3Z_{0.3}S_1T_{30}$	920	0.543	20.5	60.8	21.8	2.7
16	$IL_4Z_{0.3}S_1T_{30}$	n.d.	n.d.	<1	n.d.	n.d.	n.d.
17	$IL_5Z_{0.3}S_1T_{30}$	562	0.383	4.9	43.6	32.1	3.1
18[a]	IL_1-SS-T_{30}_1°	750	0.406	10.0	57.7	10.9	1.98
19[a]	IL_1-SS-T_{30}_2°	560	0.224	13.6	55.2	12.6	1.80
20[a]	IL_1-SS-T_{30}_3°	694	0.255	13.6	62.9	12.5	2.00
21[b]	Adenine$Z_{0.3}S_1T_{30}$	412	0.172	32.0	42.6	31.0	2.47
22[b]	OL-SS-T_{30}	600	0.453	23.8	61.3	1.64	1.16

[a] SS: sea salt. These are the 3 recycling tests. IL_1 : SS weight ratio is 1 : 1. [b] Using adenine and oak leaves (OL) as the carbon precursor.

gravimetric analyses (TGA) were performed on a Netzsch TG209-F1 apparatus at a heating rate of 10 °C min^{-1}. High resolution transmission electron microscopy (HR-TEM) and elemental mapping investigation were carried out on a JEOL JEM-2200FS instrument (JEOL GmbH, Eching, Germany). For sample preparation, one drop of the sample dispersion in ethanol was placed on a 200 mesh carbon coated copper grid and dried in air. TEM investigations were carried out at temperature around 90 K, operating at an acceleration voltage of 200 kV. All images were recorded digitally by a bottom-mounted 4k*4k CMOS camera system using low dose conditions (TemCam-F416, TVIPS, Gauting, Germany) and processed with a digital imaging processing system (EM-Menu 4.0, TVIPS, Gauting, Germany). X-ray diffraction experiments were done with a Bruker D8 diffractometer using Cu K_α radiation (λ = 0.154 nm) and a scintillation counter. XPS data were obtained on Thermo ESCALAB250 instrument with a monochromatized Alkaline source (200 W). A Controller P320 professional furnace (Nabertherm Company) was used to perform all the carbonization processes. Porcelain crucibles of 40 mm in diameter, purchased from VWR Company, were used for all the syntheses. FT-IR spectra were recorded on a Varian1000 FT-IR spectrometer. SEM image was obtained on a LEO 1550-Gemini instrument with platinum sputtering.

3. Results and discussion

Imidazolium ionic liquids (ILs) are employed as model carbon precursors in this preparation process because of their negligible vapor pressure, high thermostability and the significant presence of nitrogen in the final carbon.[6] Some recent reports have proven that a carbonization yield of 10–30 wt% at 800–1000 °C and a tunable nitrogen content in terms of the chemical design can be reached *via* an IL route.[6,9] Particularly from a structure point of view, the network-forming groups in ILs are known to build up crosslinked intermediates to improve the structural stability and correspondingly the carbonization yield. In this study ILs with different functional groups, shown in Fig. 1, are tested. In a typical run a mixture of IL, NaCl and $ZnCl_2$ in a defined weight ratio is homogeneously dissolved in water in a porcelain crucible, and then thermally treated at 250 °C in air for 2 h. This step dried the mixture and produced a solid black solution. In the presence of cyano and vinyl groups in ILs, trimerisation and the thermal polymerization occurred in parallel, which formed a crosslinked network (Fig. S1†) and favorably stabilized the carbon intermediate. Afterwards, finely grinded NaCl powder was packed directly above the black composite in the crucible. It is important to spread a few water drops to partially wet the upper NaCl surface, which becomes highly dense after thermal evaporation of water to reach a maximum space confinement. The NaCl ceiling acts here as a solid physical barrier to minimize the oxygen entrance. In addition, this confinement can retard the diffusion of the gasified decomposition products, mostly the hydrocarbons, out of the reactor, thus raising the overall carbonization yield.

The carbonization took place *via* inserting the crucible reaction in an air oven at 750 °C, *i.e.* below the melting point of NaCl (801 °C) for 30 min. At this stage, several events occur parallel. $ZnCl_2$ (m.p. ~292 °C) melts and dissolves NaCl at the bottom of the crucible, creating an ionic, homogeneous, liquid

environment for the carbon formation, in which $ZnCl_2$ initiates the carbon activation reaction. It should be clarified that although the NaCl top layer remains solid at the carbonization temperature to create a closed environment, the bottom part may join the molten salt due to the direct contact with the $ZnCl_2$/NaCl liquid mixture. Finally, the mixture was pulled out of the oven for cooling down to room temperature. The dark mixture was treated by acidic water before completely dried.

Table 1 collects characterization data of the as-synthesized carbon products. To reach a comprehensive view of the scope and applicability of this method, we systematically varied the experimental parameters, such as the amount/ratio of $ZnCl_2$ and NaCl, the carbonization time and the IL chemical structure. The S_{BET}, pore volume, carbonization yield and elemental analysis results of the final carbon product were measured and recorded. For the sake of conciseness and clearness, the carbon products derived from ILs were denoted as $IL_wZ_xS_yT_z$, in which w, x, y and z stand for the IL type, the wt% of $ZnCl_2$ with regard to IL, the wt% of NaCl, and the carbonization time at 750 °C in min, respectively. As shown in Table 1, porous carbons with large S_{BET} and high nitrogen doping were indeed received *via* this route. As a representative product, $IL_1Z_{0.30}S_1T_{30}$ (Entry 3 in Table 1), which used IL_1 as the carbon precursor and a salt mixture of 30 wt% of $ZnCl_2$ and 100 wt% of NaCl, was chosen to demonstrate the structural properties of the as-synthesized porous carbons. Fig. 2A displayed the nitrogen sorption isotherm measured at 77 K. A type-I isotherm is clearly identified and proves the dominant existence of micropores and a low fraction (<10%) of small mesopores in this carbon product. The pore volume is 0.453 $cm^3\ g^{-1}$, and a S_{BET} of 950 $m^2\ g^{-1}$ is reached. Quenched solid density functional theory (QSDFT) is used to determine the average pore size, which is in the range of 1–5 nm (Fig. S5†, red curve). It should be mentioned that in some carbon products prepared at different conditions listed in Table 1, their sorption isotherms (Fig. S5–S8†) have a broad hysteresis at high values of relative pressure. This indicates interstitial pore formation that is related to the morphology of the carbon particle aggregation discussed later. The crystalline status is characterized *via* X-ray diffraction (XRD) measurements. As shown in Fig. 2B, characteristic bands at 26°, 43° and 81° were observed, which are assigned to the (002), (100) and (110) diffraction bands of graphitic phase, respectively. The weak intensity at 81° implies that the obtained carbon lacks of a long range order, *i.e.* turbostratic.

To visualize the local atomic order, high resolution transmission electron microscopy (HR-TEM) was employed. Irregularly bent planes of various lengths are clearly visible in Fig. 2C. Scanning and transmission electron microscopy shows that $IL_1Z_{0.30}S_1T_{30}$ is composed of aggregated primary carbon nanoparticles of 20–50 nm in size (Fig. S2†). This kind of morphology of carbon particles was also observed in many other carbons in Table 1. The packing of the carbon nanoparticles densely together creates interstitial voids, responsible for the broad hysteresis at high values of relative pressure of the nitrogen sorption isotherms of some carbon products. Combustion elemental analysis reveals a high nitrogen content of 15 wt%, which is homogeneously distributed, as confirmed by elemental

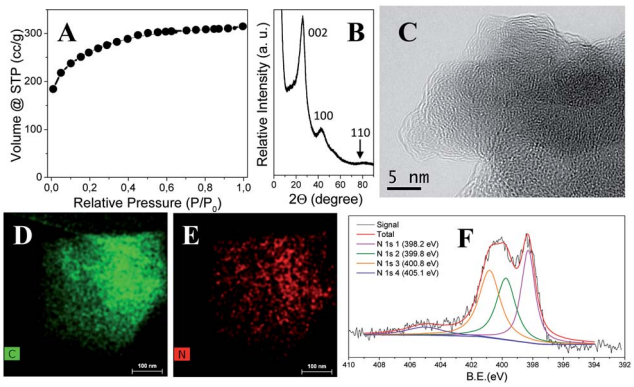

Fig. 2 Characterization of the carbon product $IL_1Z_{0.30}S_1T_{30}$: (A) nitrogen adsorption/desorption isotherm curve; (B) XRD pattern; (C) HRTEM image; (D and E) elemental mapping of carbon and nitrogen elements spectroscopy, respectively (obtained *via* SEM-EDX spectroscopy); (F) XPS spectrum of the nitrogen element.

mapping of the C and N atoms based on energy dispersive X-ray spectroscopy (EDX, Fig. 2D and E). The elemental composition of the sample surface was further checked by X-ray photoelectron spectroscopy (XPS) which depicts the presence of carbon, nitrogen and oxygen in 77.4, 14.1 and 8.5 wt%, respectively (Fig. S3†). The C and N values are close to that obtained by combustion elemental analysis method, which agrees with the EDX analysis on a homogenous distribution of the elements across the sample. A close view of the chemical states of N1s is reported in Fig. 2F. Typical binding energies of pyridinic (30.6%, 398.2 eV), pyrrolic (28.1%, 399.8 eV), quaternary – graphitic (34.0%, 400.8 eV) and oxidic-N species (7.3%, 405.1 eV) are found, proving the presence of structural nitrogen atoms intercalated in the material matrix. The existence of an oxidic-N species is a nature outcome of the carbonization process, where a small fraction of oxygen is incorporated (Fig. S4†). For the sake of completeness, control experiments under nitrogen flow were also performed (named "N_2 carbon"). In detail, the production of the sample $IL_1Z_{0.30}S_1T_{30}$ was tested under inert gas flow both with and without NaCl ceiling. The resultant N_2 carbons showed lower surface areas and pore volumes compared with the carbon obtained in air oven. Specifically 766 $m^2\ g^{-1}$ and 0.371 $cm^3\ g^{-1}$ for the salt-confined N_2 carbon and 763 $m^2\ g^{-1}$ and 0.328 $cm^3\ g^{-1}$ for the N_2 carbon without NaCl ceiling were obtained (Fig. S11 and S12,† respectively). The nitrogen content of N_2 carbons was similar to that produced in air oven (15.7 wt% for the salt-confined N_2 carbon and 14.7 wt% for the N_2 carbon without NaCl ceiling), while a slightly higher yield was observed (34.5 wt% for the salt-confined N_2 carbon and 36.4 wt% for the N_2 carbon without NaCl ceiling).

As a commonly used activation agent, the effect of $ZnCl_2$ is first investigated (Entry 1–6 in Table 1, Fig. 3A and S5†). While fixing the weight ratio of IL_1 : NaCl to 1 : 1 and varying that of $ZnCl_2$: IL_1 gradually from 0 to 100 wt%, the S_{BET} increased dramatically upon the initial addition of $ZnCl_2$ until 30 wt%. Beyond this value, it remains constant around 900 $m^2\ g^{-1}$. In comparison, the $ZnCl_2$-effect on the carbonization yield is more complex. Addition of a small portion (≤10 wt%) leads to a high

carbonization yield up to 31 wt%. Above 10 wt% of $ZnCl_2$, the carbonization yield drops. At the maximum $ZnCl_2$ addition (100 wt%) in the tests (Entry 6 in Table 1), an unfavorable low yield of only 8.4 wt% was received. The complex effect of $ZnCl_2$ is caused by the double role of $ZnCl_2$ in the carbonization process. It serves as the activation agent for the pore formation, which creates surface area and suppresses the yield. Meanwhile, it catalyzes the trimerisation of the cyano groups, which construct stable intermediates to reduce the structural fragmentation at the carbonization temperature, thus increasing the yield. Our data supports that a low fraction of $ZnCl_2$ promotes the formation of crosslinked networks, and overcompensates the weight loss caused by the activation. Too much addition of $ZnCl_2$ however makes the etching process more dominant. It is not surprising that the highest yield is found at a balanced content of $ZnCl_2$, here 10 wt% (Entry 2 in Table 1).

It is curious to find that even in the absence of $ZnCl_2$ (Entry 1 in Table 1), a porous carbon with a medium S_{BET} of 200 $m^2\ g^{-1}$ was obtained. This finding tells that in the current process, NaCl seems to be not only a salt merely to dilute the $ZnCl_2$ concentration, but also a co-activation agent, though weak. The role of NaCl (not the top NaCl layer) was thus thoroughly investigated (Entry 7–10 in Table 1, Fig. S6†). As illustrated in Fig. 3B, in the presence of 30 wt% of $ZnCl_2$, NaCl in a low fraction (30 wt%) increases the S_{BET} from 419 up to 809 $m^2\ g^{-1}$, indicating its participation in creation of porosity. Unlike $ZnCl_2$, at even higher concentrations of NaCl above 30 wt%, the pore features and the yield of the final carbon products are unaffected.

As it is true for all carbonization processes, the dwelling time is crucial, necessary means to control the physical properties of the carbons. To understand the pore development, experiments with several duration times were performed. We fixed the $IL_1 : ZnCl_2 : NaCl$ ratio to 1 : 0.3 : 1 (Entry 11–13 in Table 1, Fig. 3C and S7†). It was found that the S_{BET} increases from 813 (15 min) to 1130 $m^2\ g^{-1}$ (2 h), indicating the activation continuously introduces more porosity. In contrast, the carbonization yield decreases from 28.3 wt% to 8.4 wt% gradually due to the prolonged etching time and a possible entrance of oxygen into the reactor upon prolonged dwelling times. It is particularly worth noting that only after 15 min the S_{BET} jumps already to 812 $m^2\ g^{-1}$, implying a fast conversion of the precursor to porous carbons.

The chemical structure of ILs is important to modulate the physical property of the carbon product. Besides IL_1, four other imidazolium-based ILs (Fig. 1) with different functional groups are tested in order to reveal the relationship between the IL chemical structure and the physical feature of the as-synthesized carbons. A carbonization time of 30 min, and a starting mixture of IL : NaCl : $ZnCl_2$ in ratio of 1 : 1 : 0.3 were fixed for all runs (Entries 14–17 in Table 1, Fig. 3D and S8†).

When the cyano group in IL_1 is replaced by a methyl group in IL_2, a yield of 11.5 wt%, and a surface area of 502 $m^2\ g^{-1}$ was observed (Entry 14 in Table 1). Both values are significantly lower than that of IL_1. It proves the necessity to bring the cyano group into the IL chemical structure. Keeping the cyano functionality unchanged but substituting the vinyl with a methyl group, *i.e.* IL_3, a comparable surface area of 920 $m^2\ g^{-1}$ is obtained (Entry 15). Yet the carbonization yield drops by 9% to 20.5 wt%. As discussed above, the absence of the vinyl group fails to generate polymer chains that undergo crosslinking by the cyano groups, thus amplifying the structural fracture effect. A beneficial of IL_3 is the high nitrogen content, 22 wt%. When both cyano and vinyl groups are absent, *i.e.* IL_4, it is not astonishing to observe a carbonization yield below 1 wt% (Entry 16), a useless precursor for carbon production. Finally IL_5, bearing a cyano-containing anion was tested. A significant high nitrogen content, 32 wt% (C/N ratio of 1.4) was observed. Unfortunately, the yield is as low as 4.9 wt%. Therefore, both the vinyl and cyano groups on the cation are of key importance.

The central spirit of carrying out carbonization process without noble gas protection is to create a local oxygen-poor milieu to run oxygen-sensitive high temperature reaction. We should note that an absolute oxygen-free circumstance throughout the entire carbonization process is only idealistic. Though the top NaCl floor is dense, microchannels do exist. The reaction mixtures after 10 and 30 min were illustrated in Fig. 4. The 10 min sample displays, besides a black IL/$ZnCl_2$/NaCl bottom body, a grey top NaCl zone. This is an indication that following the initial violent decomposition of the ILs at 750 °C, the gaseous fracture compounds, majorly the carbohydrates, build up inner pressure to force the gas diffusion through the interstice in the top NaCl ceiling. The grey color thus stems from the carbon deposition of the gaseous compounds. This overpressure blocks the intrusion of the oxygen into the reactor and guarantees a true inert atmosphere at this stage. The white color of the top NaCl zone after 30 min however implies that after the initial conversion of the ILs quickly into carbons, the major reaction switches to the chemical activation by $ZnCl_2$, a relatively mild process. The high pressure built up at the initial IL thermal decomposition stage vanished, which enables the (partial) entrance of oxygen, though slow, through the microchannels in the NaCl zone into the reactor and oxidizes the formed carbons into CO or CO_2. This is in part responsible for

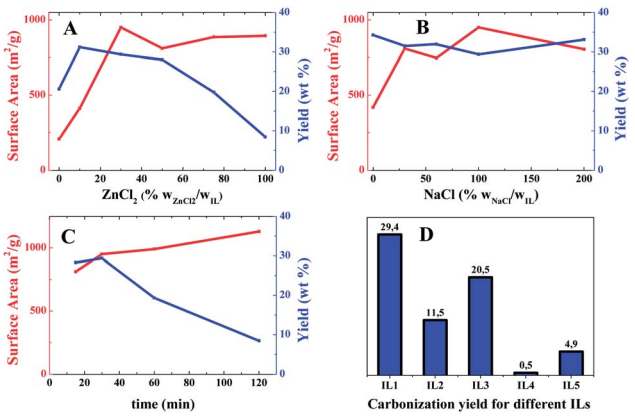

Fig. 3 The variation of the specific surface area and the carbonization yield of the nitrogen-doped porous carbons prepared at different concentrations of $ZnCl_2$ (A), NaCl (B) and different period (C). Yields from different IL precursors are also reported (D).

the low yield upon elongated carbonization (Fig. 3C). From this point of view, 30 min is an ideal reaction period to minimize the oxygen disturbance. It should be noted that due to the oxygen penetration, it may very possibly create a gradient oxidative carbon product along the sample from the top to the bottom.

The implementation of the carbonization in air without noble gas protection relies on the isolation of the reactor from the surrounding by a salt shielding below its melting point. We were motivated to modify this concept into a general and more sustainable methodology. Two key factors attract our attention, the salt mixture and the carbon precursor. In the former case, we could use sea salt to replace $ZnCl_2$/NaCl. The sea salt we tested is provided from RedSea© and it is usually used to replicate reef water system. Since the dominant fraction is NaCl, it serves favorably as the ceiling layer. Meanwhile, due to the coexistence of a small fraction of $MgCl_2$ (3.3 wt%), $CaCl_2$ (1.1 wt%) and KCl (1.0 wt%) species, it can conduct activation like $ZnCl_2$. In the test run using IL_1 as a carbon precursor, a yield of 10 wt% in 30 min and 11 wt% of nitrogen doping were obtained (Entry 18 in Table 1). The S_{BET} is 750 $m^2\ g^{-1}$, with pore volume of 0.406 $cm^3\ g^{-1}$. These exciting results prove that the natural sea salt can replace the NaCl/$ZnCl_2$ binary system. An additional merit of sea salt is the easy recyclability due to the identical salt composition all over the reactor. In a 3-recycle test, the sea salt preserves well its shielding and activation function (Entry 19 and 20 in Table 1 and Fig. S9†).

In the latter case to replace ILs as carbon precursor, we were motivated to employ natural raw materials. Nucleobases such as adenine, possess a high atomic N/C ratio, high oxidation stability, and suitable atomic N–C–N bonding motifs. They can be isolated from nature in larger quantities, and have been explored for functional carbon synthesis very recently.[1] Here adenine was tested in the $ZnCl_2$/NaCl system. The formed nitrogen-doped porous carbons showed a high carbonization yield of 32 wt%, a high nitrogen content of 31 wt% and a satisfactory S_{BET} of 412 $m^2\ g^{-1}$ (Entry 21 in Table 1, Fig. S10†). In addition to nucleobase, biomass is also applied. For example, the oak leaves have been successfully converted to porous carbon using sea salt (Entry 22 in Table 1, and Fig. S13†). As shown in Fig. 5, the oak leaves were collected and grinded with the sea salt into fine powders to reach a homogeneous mixture. Upon the carbonization procedure mentioned above (see Section 2.5), fine carbon powders with S_{BET} of 600 $m^2\ g^{-1}$ were achieved. The nitrogen sorption isotherm is shown in Fig. 5D. Beside a significant amount of micropores, the sample contains a considerable fraction of mesopores. The pore volume is 0.45 $cm^3\ g^{-1}$, which contains a mesopore volume of 0.33 $cm^3\ g^{-1}$. Its nitrogen content is relatively low, only 1.6 wt%, which comes from the proteins existing in the oak leaves (elemental analysis of fresh oak leaves showed nitrogen content of 1.1 wt%).

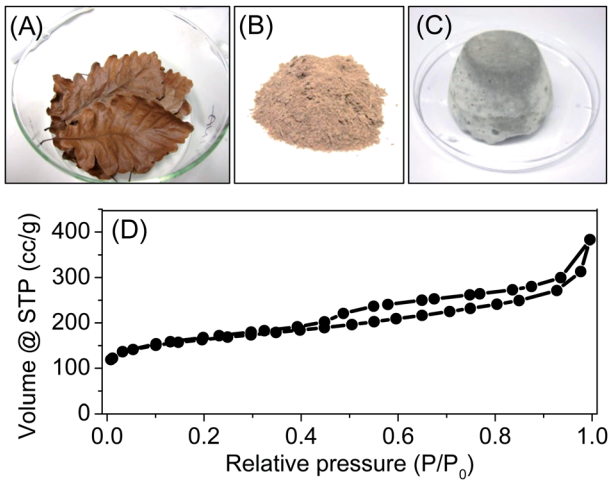

Fig. 5 (A–C) Photographs of pristine oak leaves, grinded powder of oak leaves and sea salt, and the carbonization mixture after 30 min at 750 °C. (D) N_2 sorption isotherm of the carbon prepared from the oak leaves.

4. Conclusions

In summary, we introduced a general synthetic route to produce nitrogen-doped porous carbons with high surface area and

Fig. 4 Illustration of the reaction mixture after 10 and 30 min. The two photographs on the right side show the reaction mixture at 10 and 30 min.

tunable nitrogen content in an air oven. This conceptually straightforward production procedure is easy to implement. Not only the salt can be replaced by recyclable sea salt, but also the carbon precursor is accessible from natural sources, thus pointing out a more sustainable way for the nitrogen-doped carbon production. Furthermore, the method is expected to be able to conduct many other high temperature chemical processes in air instead of under inert gas environment, for instance, the preparation of metal nanoparticles, and the synthesis of metal carbide or nitride.

Acknowledgements

F.P. thanked the CRC 951 of the German research Council and the Joint Lab for Structural Research within IRIS Adlershof for funding. J.Y. thanked Prof. M. Antonietti and Dr N. Fechler for helpful discussion. This work is financialized by the Max Planck Society and the People Programme (Marie Curie Actions) of the European Union's Seventh Framework Programme FP7/2007–2013 under REA grant no. 289347.

Notes and references

1 W. Yang, T.-P. Fellinger and M. Antonietti, *J. Am. Chem. Soc.*, 2010, **133**, 206–209.
2 K. Gong, F. Du, Z. Xia, M. Durstock and L. Dai, *Science*, 2009, **323**, 760–764.
3 D. P. Kim, C. L. Lin, T. Mihalisin, P. Heiney and M. M. Labes, *Chem. Mater.*, 1991, **3**, 686–692.
4 Y. Men, M. Siebenburger, X. Qiu, M. Antonietti and J. Yuan, *J Mater. Chem. A*, 2013, **1**, 11887–11893.
5 J. P. Paraknowitsch, A. Thomas and M. Antonietti, *J. Mater. Chem.*, 2010, **20**, 6746.
6 J. S. Lee, X. Wang, H. Luo, G. A. Baker and S. Dai, *J. Am. Chem. Soc.*, 2009, **131**, 4596–4597.
7 Z.-S. Wu, S. Yang, Y. Sun, K. Parvez, X. Feng and K. Müllen, *J. Am. Chem. Soc.*, 2012, **134**, 9082–9085.
8 W. Li, Z. Zhang, B. Kong, S. Feng, J. Wang, L. Wang, J. Yang, F. Zhang, P. Wu and D. Zhao, *Angew. Chem., Int. Ed.*, 2013, **52**, 8151–8155.
9 J. P. Paraknowitsch, J. Zhang, D. Su, A. Thomas and M. Antonietti, *Adv. Mater.*, 2010, **22**, 87–92.
10 S. Soll, T.-P. Fellinger, X. Wang, Q. Zhao, M. Antonietti and J. Yuan, *Small*, 2013, **9**, 4135.
11 D. Kuzmicz, S. Prescher, F. Polzer, S. Soll, C. Seitz, M. Antonietti and J. Yuan, *Angew. Chem., Int. Ed.*, 2014, **53**, 1062–1066.
12 P. Zhang, J. Yuan, T.-P. Fellinger, M. Antonietti, H. Li and Y. Wang, *Angew. Chem., Int. Ed.*, 2013, **52**, 6028–6032.
13 Q. Zhao, T.-P. Fellinger, M. Antonietti and J. Yuan, *J. Mater. Chem. A*, 2013, **1**, 5113–5120.
14 J. Balach, H. Wu, F. Polzer, H. Kirmse, Q. Zhao, Z. Wei and J. Yuan, *RSC Adv.*, 2013, **3**, 7979–7986.
15 K. K. R. Datta, V. V. Balasubramanian, K. Ariga, T. Mori and A. Vinu, *Chem.–Eur. J.*, 2011, **17**, 3390–3397.
16 W. Luo, B. Wang, C. G. Heron, M. J. Allen, J. Morre, C. S. Maier, W. F. Stickle and X. Ji, *Nano Lett.*, 2014, **14**, 2225–2229.
17 D. Kuzmicz, P. Coupillaud, Y. Men, J. Vignolle, G. Vendraminetto, M. Ambrogi, D. Taton and J. Yuan, *Polymer*, 2014, **55**, 3423–3430.
18 M.-R. Gao, X. Cao, Q. Gao, Y.-F. Xu, Y.-R. Zheng, J. Jiang and S.-H. Yu, *ACS Nano*, 2014, **8**, 3970–3978.
19 P. Chen, T.-Y. Xiao, Y.-H. Qian, S.-S. Li and S.-H. Yu, *Adv. Mater.*, 2013, **25**, 3192–3196.
20 G.-P. Hao, W.-C. Li, D. Qian and A.-H. Lu, *Adv. Mater.*, 2010, **22**, 853–857.
21 D. Wu, Z. Li, M. Zhong, T. Kowalewski and K. Matyjaszewski, *Angew. Chem., Int. Ed.*, 2014, **53**, 3957–3960.
22 W. H. Suh, J. K. Kang, Y.-H. Suh, M. Tirrell, K. S. Suslick and G. D. Stucky, *Adv. Mater.*, 2011, **23**, 2332–2338.
23 C. Galeano, J. C. Meier, V. Peinecke, H. Bongard, I. Katsounaros, A. A. Topalov, A. Lu, K. J. J. Mayrhofer and F. Schüth, *J. Am. Chem. Soc.*, 2012, **134**, 20457–20465.
24 J. Yuan, C. Giordano and M. Antonietti, *Chem. Mater.*, 2010, **22**, 5003–5012.

